Even harmonic pulse train generation by cross-polarization-modulation seeded instability in optical fibers

Julien Fatome,[1] Ibrahim El-Mansouri,[1] Jean-Luc Blanchet,[1] Stéphane Pitois,[1] Guy Millot,[1] Stefano Trillo,[2] and Stefan Wabnitz[1,3,*]

[1]*Laboratoire Interdisciplinaire Carnot de Bourgogne, UMR 6303 CNRS/Université de Bourgogne, Dijon 21078, France*
[2]*Dipartimento di Ingegneria, Università di Ferrara, Via Saragat 1, Ferrara 44122, Italy*
[3]*Department of Information Engineering, Università di Brescia, Brescia 25123, Italy*
**Corresponding author: stefano.wabnitz@ing.unibs.it*

Received October 1, 2012; accepted November 9, 2012;
posted November 12, 2012 (Doc. ID 177297); published December 12, 2012

We show that, by properly adjusting the relative state of polarization of the pump and of a weak modulation, with a frequency such that at least one of its even harmonics falls within the band of modulation instability, one obtains a fully modulated wave at the second or higher even harmonic of the initial modulation. An application of this principle to the generation of an 80 GHz optical pulse train with high extinction ratio from a 40 GHz weakly modulated pump is experimentally demonstrated using a nonzero dispersion-shifted fiber in the telecom C band.

OCIS codes: 060.5530, 060.4370, 190.4380, 190.0190.

1. INTRODUCTION

Modulation instability (MI) of a CW solution of the scalar nonlinear Schrödinger equation (NLSE) that describes pulse propagation in a weakly dispersive and nonlinear medium (e.g., an optical fiber) was first discovered by Bespalov and Talanov [1] for light waves in nonlinear liquids and by Benjamin and Feir for deep water waves [2] and extended to coupled wave models by Berkhoer and Zakharov [3] (for a recent review see also [4]). For scalar wave propagation, the MI-induced breakup of the CW in the anomalous group-velocity dispersion (GVD) leads to the formation of a train of pulses at the repetition rate set by the frequency of an initial modulation. Exact time-periodic solutions of the NLSE provide a full analytical description of the MI process past the initial stage of growth of the sidebands [5–7]. In a simpler approach, most of the noteworthy features of the nonlinear stage of MI (e.g., the homoclinic structure) are also correctly captured by truncations to few Fourier modes [8,9]. A remarkable feature of the nonlinear dynamics of the MI process is that the wave evolution is generally periodic both in the time as well as in the propagation coordinate (the spatial periodicity is also referred to as Fermi–Pasta–Ulam recurrence), as also confirmed experimentally [10]. In the case of noise-activated MI, the modulation frequency that is selected corresponds to the peak of the gain curve corresponding to the nonlinear phase matching. In the intermediate situation when multiple unstable modulations are present at the input, a nonlinear superposition of the periodic evolutions is obtained, which may lead to the generation of different pulse trains with harmonic frequencies at different points along the propagation coordinate [5,7]. Indeed, it was numerically pointed out [11] and experimentally observed recently [12] that harmonic pulse trains may be generated at different distances even when a single sufficiently slow modulation is present at the input. Seeding of these trains is produced by the generation of all of the harmonics at the point of maximum temporal compression of the pulse train at the fundamental frequency.

The most direct extension of the NLSE is provided by its vector counterpart or VNLSE where two polarization components are incoherently coupled via nonlinear cross-phase modulation. Such a situation holds for instance in a birefringent fiber whenever the coherent terms can be averaged to zero as they are fast-rotating terms. In particular, in this case, the efficient conversion of a modulated wave into a nearly sinusoidally modulated wave at harmonic frequencies has been previously demonstrated by means of MI induced by multiple four-wave mixing in the case of a normally dispersive, highly birefringent fiber at visible wavelengths [13]. In this paper we rather focus on the VNLSE in the anomalous GVD regime, and in particular we are interested in the situation where the self- and cross-induced nonlinear terms have the same weight (Manakov system [14]), which applies to the relevant practical case of telecommunication fiber-optic links with random birefringence [15]. MI for the VNLSE has been known for a long time [16], and its multiply periodic solutions representing the homoclinic extension of the unstable CW solutions have been obtained by methods based on the inverse scattering transform method [17–22]. These methods have been also recently applied to obtaining deterministic rogue wave (or time and space localized) solutions of the VNLSEs, which may also be coupled with bright and dark soliton solutions [23,24].

In this work we point out and experimentally demonstrate an interesting and, to the best of our knowledge, yet unreported property of the MI associated with polarized waves. Namely, whenever the CW and its modulation are orthogonally polarized at the input of an optical fiber, the projection of the initial modulation on the spatially unstable sidebands is initially zero so that no MI is activated at the fiber input. Nevertheless, MI is progressively induced upon propagation on the CW through cross-polarization modulation (XPolM). As a result, the breakup of the CW into a pulse train is still observed, with, however, two important differences with respect to the scalar case; namely, (i) only even harmonics of the initial modulation are present in the pulse train and (ii) the CW pedestal that accompanies MI-induced pulse trains in the scalar case is fully suppressed in the vector case, thus permitting in principle to achieve very large extinction ratios. The application of this effect to the all-optical generation of an 80 GHz high-contrast pulse train from a cross-polarized 40 GHz electro-optical weak modulation is experimentally demonstrated.

2. THEORY

The propagation of a polarized optical field in randomly birefringent optical fibers with relatively low polarization mode dispersion (PMD) may be described in dimensionless units in terms of the VNLSE [9]:

$$i\frac{\partial u}{\partial z}+\frac{1}{2}\frac{\partial^2 u}{\partial t^2}+(|u|^2+|v|^2)u=0,$$
$$i\frac{\partial v}{\partial z}+\frac{1}{2}\frac{\partial^2 v}{\partial t^2}+(|v|^2+|u|^2)v=0, \quad (1)$$

Here z and t denote the distance and retarded time (in the frame traveling at the common group velocity) coordinates, respectively, whereas u and v indicate the two orthogonal polarization components of the field. Although we explicitly deal with the VNLSE in the integrable Manakov case, we point out that the phenomenon described below occurs for a generic ratio of the cross-to-self-phase modulation coefficients as well. Let us consider the nonlinear evolution of a weakly modulated CW pump, which reads at $z=0$ as

$$u(z=0,t)=u_0+\varepsilon_u\exp(i\varphi_u)\cos(\Omega t),$$
$$v(z=0,t)=v_0+\varepsilon_v\exp(i\varphi_v)\cos(\Omega t), \quad (2)$$

where we take real carrier amplitudes u_0, v_0, with $u_0^2+v_0^2=1$; $\varepsilon_{u,v}$, $\phi_{u,v}$, and Ω are the initial modulation amplitudes, phases, and frequency, respectively.

As it is well known, in the anomalous GVD regime MI of the CW solution of Eq. (1) occurs for a perturbation in Eq. (2) with the same state of polarization of the pump (i.e., whenever $\phi_u=\phi_v$) and modulation frequency Ω in the range $0\le\Omega\le\Omega_c$, where $\Omega_c=2$. The nonlinear evolution of the initial condition Eq. (2) leads to the development of a pulse train at the fundamental frequency Ω, that is with temporal period $T=2\pi/\Omega$. Such a pulse train exhibits a spatial recurrent behavior in z; i.e., it periodically forms and then returns back to the initial CW along the propagation distance.

Moreover, whenever the harmonics of the initial modulation frequency (with, say, amplitude u_m for the mth harmonic at frequency $m\Omega$) are also unstable (i.e., if $m\Omega\le\Omega_c$ with $m>1$), the nonlinear evolution of the weakly modulated pump Eq. (2) may also lead to the development of harmonic pulse trains, i.e., with periods $T_m=2\pi/(m\Omega)$. It is remarkable that these harmonic pulse trains typically appear at intermediate distances among the points of formation of the pulse trains at fundamental frequency Ω. In this way, by simply adjusting the input pump power, one may select at the fiber output a particular repetition rate among the fundamental and its harmonics.

The behavior of the solutions of the VNLSE reproduces the scalar situation in the case of input modulations with the same state of polarization of the pump. This is shown in Fig. 1, which displays the spatiotemporal evolution of the amplitude $|u|$, when the linearly polarized CW pump oriented at 45 deg from the two degenerate axes of birefringence of the fiber (i.e., with $u_0^2=v_0^2=1/2$) is perturbed by an initial in-phase and parallel amplitude modulation with frequency $\Omega_1=0.8718$ (so that $2\Omega_1<\Omega_c$) and $\varepsilon_u=\varepsilon_v=10^{-2}u_0$, $\phi_u=\phi_v=0$. As can be seen from Fig. 1, a primary pulse train with period T forms at approximately $z=6$ and $z=20$. At these distances, all harmonics of the fundamental frequency Ω are generated. Figure 1 also shows that, near $z=13$, a harmonic secondary pulse train with period $T_2=T/2$ is formed. Clearly, though the second harmonic 2Ω is absent in the input perturbation Eq. (2), such a component is generated along the fiber whenever the fundamental pulse train is formed, as shown by Fig. 2(a), which provides the evolution of the amplitude of the first four (positive) harmonics $m\Omega$, $m=1,2,3,4$.

Note also from Fig. 2(a) that the secondary train is composed of even harmonics only. Because of the symmetry of the field spectrum about the pump carrier frequency, sidebands with opposite frequency detuning from the pump have equal amplitudes. The evolution of the orthogonal polarization component amplitude $|v|$ is not reported here since it is identical to $|u|$. The generation of the harmonic pulse train may be controlled by varying the relative phase between the CW pump and the input modulation: as was shown in [11], with $\Omega=\Omega_1$ and in the case of quadrature modulation, that is whenever $\phi_u=\phi_v=\pi/2$, only the pulse train at the fundamental frequency is formed.

The situation may be radically different in the case of input modulations with a different state of polarization from the pump. As is shown in Figs. 2(b) and 3, for orthogonally polarized pump and sidebands ($\phi_u=-\phi_v=\pi/2$), the pulse train at the fundamental frequency $\Omega=\Omega_1$ is no longer generated:

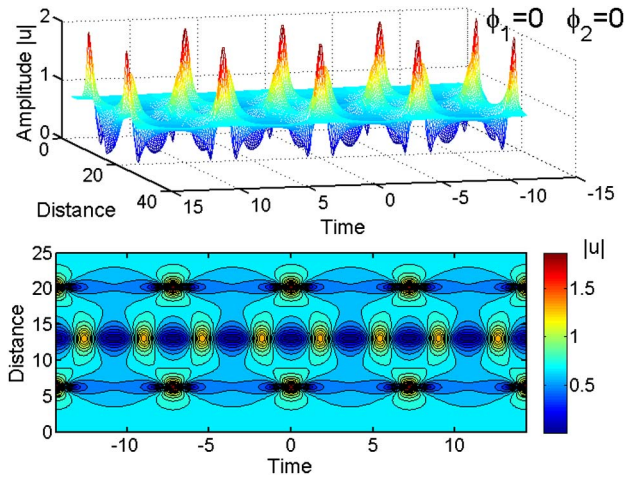

Fig. 1. (Color online) Surface and contour plots of the evolution with distance of the field amplitude $|u|$. Initial in-phase amplitude modulation with $\Omega=\Omega_1=0.8718$, $\varepsilon_u=\varepsilon_v=10^{-2}u_0$, $\phi_u=\phi_v=0$.

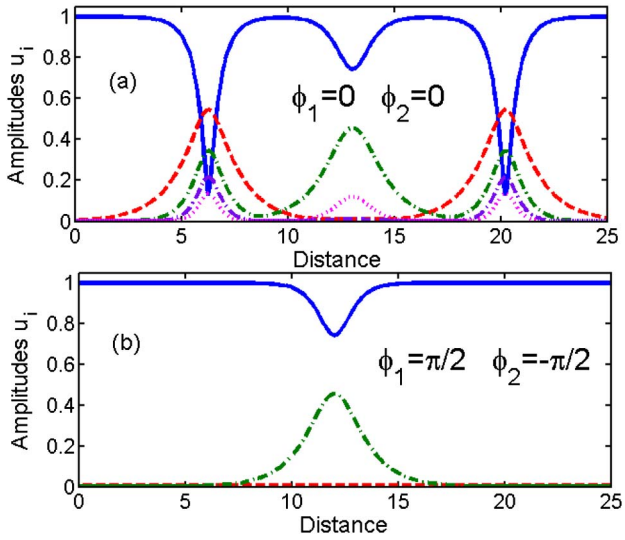

Fig. 2. (Color online) Evolution with distance z of the amplitudes of the pump and its harmonics u_i: (a) initial in-phase and parallel modulation, CW pump (blue solid curve), the sideband at frequency shift $\Omega = +\Omega_1$ from the pump (red dashed curve), its second harmonic at $\Omega = +2\Omega_1$ (green dotted-dashed curve with a peak near $z = 13$), third harmonic $\Omega = +3\Omega_1$ (violet dotted–dashed curve), and fourth harmonic $\Omega = +4\Omega_1$ (pink dotted curve) corresponding to the case in Fig. 1; (b) initial modulation orthogonal to the pump.

only a pulse train at the second-harmonic frequency $2\Omega_1$ is observed. Again the evolution of the orthogonal amplitude $|v|$ is the same as the evolution of $|u|$ and is not reported here. Unlike the case of modulations with the same state of polarization as the pump, whenever the pump and the sidebands are orthogonally polarized, the evolutions of the two polarization amplitudes are unaffected by their relative phase. In fact, the contour plot of the pulse amplitude $|u|$ that is obtained with $\phi_u = 0$, $\phi_v = \pi$ is the same as that of Fig. 3 where $\phi_u = -\phi_v = \pi/2$.

In order to better characterize the amplification process of the modulation in the cross-polarized mode of the seed and its nonlinear evolution, we have numerically integrated Eqs. (1) with fixed modulation amplitude and phase $\phi_u = 0$, $\phi_v = \pi$ by varying the value of the sideband frequency detuning Ω. The surface plot in Fig. 4(a) refers to a modulation frequency

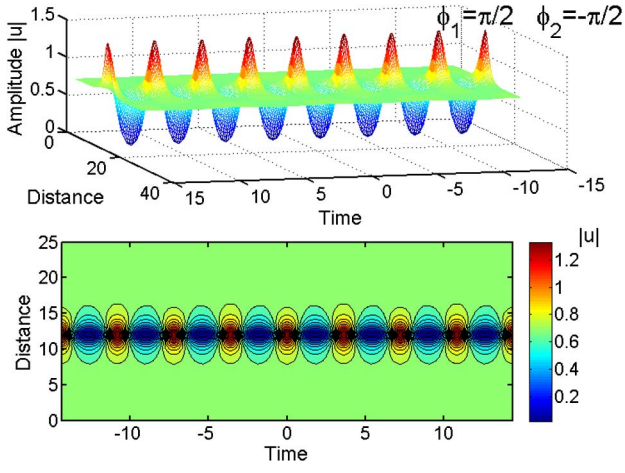

Fig. 3. (Color online) Same as Fig. 1, with a quadrature modulation that is orthogonal to the pump, i.e., with $\phi_u = -\phi_v = \pi/2$.

$\Omega = \sqrt{2}$, which corresponds to peak MI gain for parallel modulations: as can be seen, the MI gain vanishes for orthogonal modulations. Indeed, Fig. 4(a) shows that there is no exponential growth of the initial modulation. Conversely, only periodic small oscillations are observed. On the other hand, as shown in Figs. 4(b) and 4(c), harmonic pulse trains at frequency 2Ω are always observed as soon as $\Omega \le 1$, owing to the MI of the second harmonic of the initial modulation. Moreover, the modulation depth and the amplitude of the generated pulse train at the second-harmonic repetition rate grows larger as the sideband detuning is progressively reduced below $\Omega = 1$.

As can be seen from Fig. 5(a), whenever $\Omega = 0.5$, the amplitude of the CW pump vanishes at the point of maximum pulse compression, which means that an ideal infinite extinction ratio is achieved. This can be explained as follows. In the theory of scalar nonlinear MI, the normalized modulation frequency $\Omega = 1$ is the frequency that allows complete depletion of the pump toward the modulation and its harmonics. In fact, while a normalized modulation frequency $\Omega = \sqrt{2}$ gives the maximum rate of conversion in the initial stage since it corresponds to nonlinear phase matching, such a rate is rapidly saturated by pump depletion, which tends to drive the mixing interaction out of phase matching (the new phase-matching frequency shifts toward lower frequencies). Conversely, a modulation with lower frequency, though being initially amplified at a lower rate, is progressively tuned toward nonlinear phase matching by the pump depletion, the optimal condition corresponding indeed to a frequency $\Omega = 1$ [8,9]. In the cross-polarization case examined here, this condition is realized when the second harmonic of the input modulation frequency is equal to $\Omega = 1$, which results indeed into an optimal input frequency $\Omega = 0.5$. In addition, Figs. 4(c), 5(b), and 6(b) reveal that, whenever $\Omega < 0.5$, in addition to the second-harmonic pulse train, a secondary pulse train is formed at the fourth-harmonic frequency 4Ω, due to the parametric amplification owing to MI of the fourth harmonic. In particular, Fig. 5(b) shows that, for $\Omega = 0.4$, the second-harmonic pulse train that is formed at around $Z = 14$ only contains even harmonics of the initial modulation, whereas the fourth-harmonic pulse

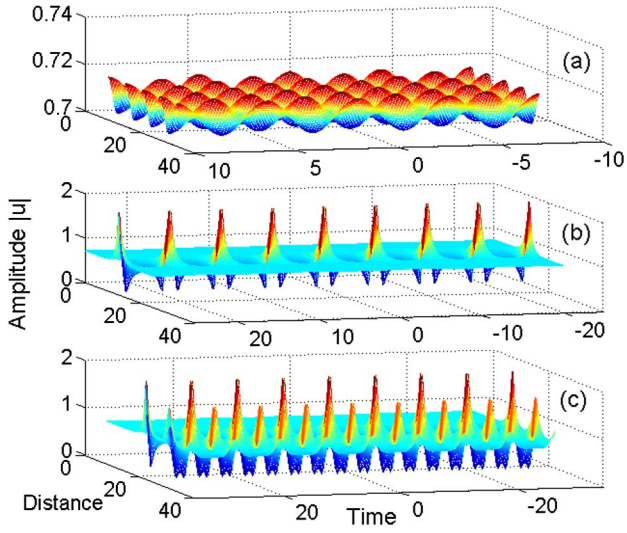

Fig. 4. (Color online) Surface plot of the amplitude $|u|$ with orthogonal input pump and sidebands $\phi_u = 0$, $\phi_v = \pi$ and the different sideband modulation frequencies: (a) $\Omega = \sqrt{2}$, (b) $\Omega = 0.5$, and (c) $\Omega = 0.4$.

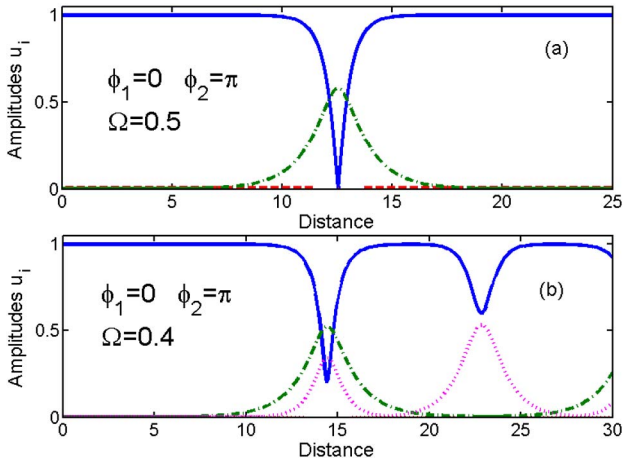

Fig. 5. (Color online) Same as in Fig. 2, with reference to the cases in Fig. 4 with (a) $\Omega = 0.5$ and (b) $\Omega = 0.4$.

train that forms at $Z = 23$ only contains the fourth harmonic and its multiples.

The physical mechanism that leads to the generation of pulse trains at repetition rates equal to even harmonics of the initial modulation is that orthogonal perturbations affect the CW pump propagation through cross-phase modulation, which implies that the perturbation acts on the pump through its squared modulus. Therefore, nothing is expected to change with respect to previous cases if we rotate both the sidebands and the input pump linear polarization by $\pi/4$ so that we set in Eqs. (2) $u_0^2 = 1$, $v_0^2 = 0$ and $\varepsilon_u = 0$, $\varepsilon_v = 0.01$, $\phi_u = \phi_v = 0$. The corresponding nonlinear evolution of the MI is shown in Fig. 7, where we display the surface plots of the amplitudes $|u|$ and $|v|$ of both polarization components of the field, with $\Omega = 1/\sqrt{2} = 0.707$. As expected, even though the initial modulation in Eq. (2) only involves sidebands at frequency Ω, also in this case even harmonics of the input modulation are created along the fiber by XPolM in the same polarization state of the pump wave.

This case allows us to get a deeper insight into the XPolM-activated MI process. In fact, it might be surprising that new frequencies are generated onto mode u through a modulation impressed onto an orthogonal mode (v), which interacts only through the cross-phase modulation. In order to gain a better

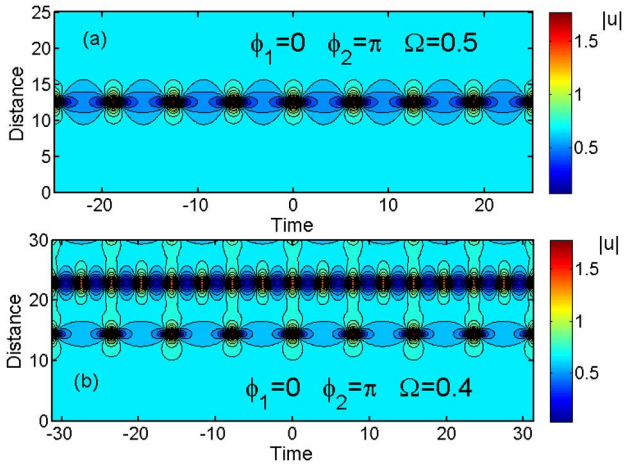

Fig. 6. (Color online) Contour plots as in Fig. 4, with (a) $\Omega = 0.5$ and (b) $\Omega = 0.4$.

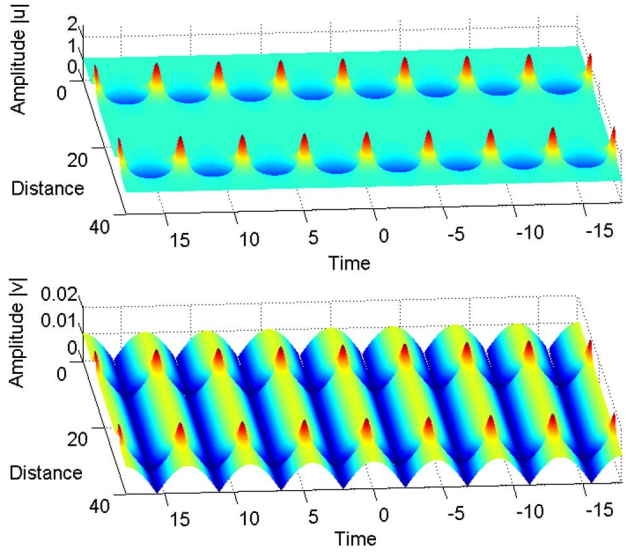

Fig. 7. (Color online) Surface plots of the temporal evolution with distance of the field amplitudes $|u|$ and $|v|$, exhibiting recursive behavior. Input pump in the u mode ($u_0 = 1$, $v_0 = 0$) and modulation at frequency $\Omega = 1/\sqrt{2} = 0.707$ in the v mode, $\varepsilon_u = 0$, $\varepsilon_v = 10^{-2}$, $\phi_u = \phi_v = 0$. Note also the different vertical scale.

understanding of the underlying mechanisms, it is convenient to consider a finite-number mode truncation [9] by inserting in Eq. (1) the expressions $u = u_0(z) + u_2(z)\exp(i2\Omega t) + u_2(z)\exp(-i2\Omega T)$ and $v = v_1(z)\exp(i\Omega t) + v_{-1}(z)\exp(-i\Omega t)$. By grouping terms of same frequency, one obtains a closed set of ordinary differential equations (ODEs) for the five Fourier modal amplitudes, which permits us to isolate the mixing terms that are responsible for the generation of even harmonic frequency $(\omega_0 \pm 2\Omega)_u$ (henceforth the subscript indicates the mode to which the frequency belongs, while the frequency Ω within parenthesis is intended to be in real-world units for dimensional consistency with the pump carrier frequency ω_0). We find that the latter are indeed generated as $(\omega_0 + 2\Omega)_u = (\omega_0 + \Omega)_v - (\omega_0 - \Omega)_v + (\omega_0)_u$ and $(\omega_0 - 2\Omega)_u = (\omega_0 - \Omega)_v - (\omega_0 + \Omega)_v + (\omega_0)_u$, which entails two independent photon processes: (i) a pair at $(\omega_0 + 2\Omega)_u$ and $(\omega_0 - \Omega)_v$ is generated by annihilating a pair at $(\omega_0 + \Omega)_v$ and $(\omega_0)_u$, and (ii) a pair at $(\omega_0 - 2\Omega)_u$ and $(\omega_0 + \Omega)_v$ is generated by annihilating a pair at $(\omega_0 - \Omega)_v$ and $(\omega_0)_u$. Overall, the simultaneous occurrence of these two processes creates two photons in the even sidebands $(\omega_0 \pm 2\Omega)_u$ at the expense of two photons of the sole input pump at $(\omega_0)_u$, while leaving unchanged the number of photons in the orthogonal signal [i.e., $(\omega_0 \pm \Omega)_v$]. This description turns out to be consistent with the pure phase interaction between the pump mode u and the signal mode v. However, once the even modulation sidebands at $(\omega_0 \pm 2\Omega)_u$ are created through this double process, they are primarily amplified through the standard (scalar) mixing interaction, which is behind seeded scalar MI, i.e., the direct generation of a photon pair at $(\omega_0 + 2\Omega)_u$ and $(\omega_0 - 2\Omega)_u$ at the expense of two photons at pump frequency $(\omega_0)_u$. This explains why the XPolM mechanism is only efficient when the normalized modulation frequency 2Ω falls within the bandwidth of scalar MI ($\Omega < 2$ in normalized units). At this point, we may also emphasize that such a complicated multiphoton process could remarkably lead to the spatially periodic evolution of the amplification of even harmonic modulations, as is

shown in Fig. 7. In this sense, because of the competition between the XPolM and the scalar MI effects, the occurrence of XPolM–MI could also be viewed as a stabilization of the input pump against its decay into sideband pairs with the same polarization owing to spontaneous MI (i.e., due to amplification of noise). However, over long propagation distances (i.e., several spatial periods of the amplification of cross-polarized even harmonics, well beyond the length used in the experiment), the spontaneous MI of the pump is expected to hamper the recurrence of the seeded process, a problem that remains far beyond the scope of this paper and that will be addressed in details in a future study.

From a practical point of view, the interest of using cross-polarized sidebands in optical fibers is twofold. First of all, orthogonal modulations may be exploited whenever one wants to avoid the MI altogether. In fact, pump MI is fully suppressed as long as $\Omega \geq 1$ (as opposed to $\Omega \geq 2$ for the case of parallel sidebands). In addition, Fig. 1 shows that, even when $\Omega < 1$, the harmonic pulse train only develops after a distance that is more than twice the distance for the development of the fundamental pulse train. Thus, if one wants to avoid MI, the limitation to the maximum fiber length (or pump power) is substantially mitigated. On the other hand, using cross-polarized sidebands leads to the possibility to impress a full modulation onto a CW laser at even multiples (2Ω–4Ω) of the initial frequency detuning Ω of the seed. By full modulation we mean that a large extinction ratio is obtained thanks to the absence of the residual CW pedestal that always accompanies the fundamental pulse train generated by scalar MI, clearly visible in Fig. 2(a). Note also from Figs. 4(c), 5(b), and 6(b) that the quadrupling of the initial modulation frequency is observed at the relatively large distance $z = 23$. This distance can be reduced substantially by increasing the relative strength of the initial modulation. See for example Fig. 8, where, as in Fig. 7, we have set in Eq. (2) $u_0^2 = 1$, $v_0^2 = 0$ and $\varepsilon_u = 0$, $\phi_u = \phi_v = 0$ but we increased the orthogonal input modulation amplitude by ten times to have $\varepsilon_v = 0.1$: as can be seen in Fig. 8, in this case frequency doubling is observed at $z = 8$ (down from $z = 14$ with $\varepsilon_v = 0.01$) and frequency quadrupling at $z = 14$ (down from $z = 23$ with $\varepsilon_v = 0.01$).

By turning from dimensionless to real units, the input pump power P reads as $P = (\gamma Z_c)^{-1}$, where $\gamma = \omega_0 n_2/(cA_{\text{eff}})$ is the fiber nonlinear coefficient, ω_0 is the pump carrier frequency, n_2 is the nonlinear refractive index, and A_{eff} is the effective core area of the fiber. Moreover, in Eq. (1), $z = Z/Z_c$ and $t = T/T_c$, where Z and T are distance and time in real-world units, the dispersion length $Z_c = T_c^2/|\beta_2|$, $T_c = \Omega/(2\pi\Delta\nu)$, β_2 is the fiber chromatic dispersion at the pump frequency, and $\Delta\nu$ is the real-world frequency of the input modulation. For instance, taking the nonlinear coefficient of a highly nonlinear fiber $\gamma = 12\ \text{W}^{-1}\,\text{km}^{-1}$ and $P = 400$ mW, one obtains $Z_c = 208$ m so that the distance $z = 14$ as in Figs. 5 and 6 corresponds to an effective fiber length $Z = 2.9$ km. With $\beta_2 = -12\ \text{ps}^2/\text{km}$, one obtains $T_c = 1.6$ ps so that $\Omega = 0.4$ corresponds to $\Delta\nu = 40$ GHz. In Section 3, we show that the observation of the phenomenon can also be carried out in dispersion-shifted low-PMD fiber with standard nonlinear coefficient.

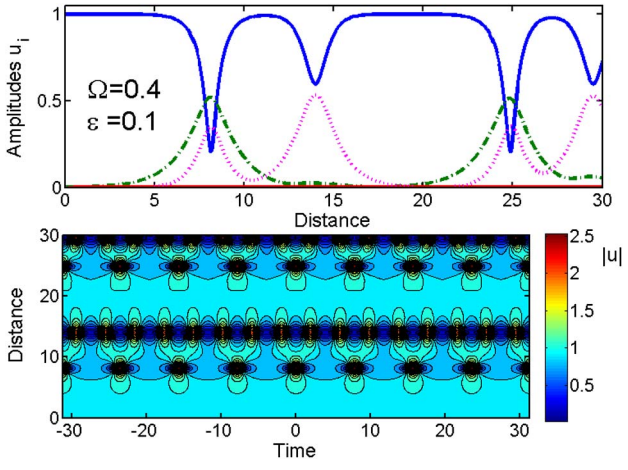

Fig. 8. (Color online) CW and sideband (a) amplitudes and (b) contour plot in the u mode with $\Omega = 0.4$, $\varepsilon_u = 0$, $\varepsilon_v = 10^{-1}$, $\phi_u = \phi_v = 0$.

3. EXPERIMENTS

In this section we will confirm the theoretical predictions of Section 2 and experimentally show that one can produce a fully modulated periodic pulse train at the repetition rate of 80 GHz that is well beyond the capabilities of electrically driven modulators. The experimental setup is sketched in Fig. 9. A continuous pump wave is generated by a laser diode emitting polarized light at 1555 nm. A first intensity modulator driven by a 40 GHz RF clock is then used to generate sidebands on either side of the pump frequency. Two of these sidebands will be used in the second part of this setup to generate the sinusoidal signal wave.

In order to inhibit the stimulated Brillouin scattering (SBS) effect that may occur in the optical fiber, a phase modulator is inserted into the setup so as to increase the spectral linewidth of the pump wave. The phase modulator is driven by a 28 dBm 85 MHz RF signal, thus enabling us to work at relatively high pump powers, still being far below the SBS threshold. Moreover, in order to increase significantly the peak power involved in our experiment while keeping an average power below the SBS threshold, we have temporally carved the emitting light beam thanks to a second intensity modulator. More precisely, a 250 ps square pulse train at a repetition rate of 4 GHz (1/10 of the RF clock frequency of the first intensity modulator) is carved into the light beam thanks to a RF sequence of 4 bits (0010) so as to create a block of 10 initial signal periods with a duty cycle of 1∶4. We would like to emphasize that such pulses provide a quasi-CW condition since the expected temporal modulation period will be around 12.5 ps. The light beam is then amplified and split owing to an erbium-doped fiber amplifier and a 50∶50 coupler, respectively. At this stage, pump and signal waves are spectrally separated by means of two programmable optical filters (Finisar Waveshaper) while their polarizations are independently adjusted by means of polarization controllers so as to emerge orthogonally (or parallel) polarized. Finally, pump and signal waves are recombined before their amplification and injection into the optical fiber. The optical fiber used in our experiment was provided by Prysmian Group and has a length of 5100 m, a chromatic dispersion of $D = 4.7\ \text{ps/nm/km}$, a dispersion slope of $S = 0.05\ \text{ps/nm}^2\text{/km}$, and a nonlinear coefficient $\gamma = 1.7\ \text{W}^{-1}\,\text{km}^{-1}$. This fiber has a very low PMD equal to $0.02\ \text{ps/km}^{1/2}$. After propagation, the resulting signal was analyzed both in spectral and temporal domains by means of an

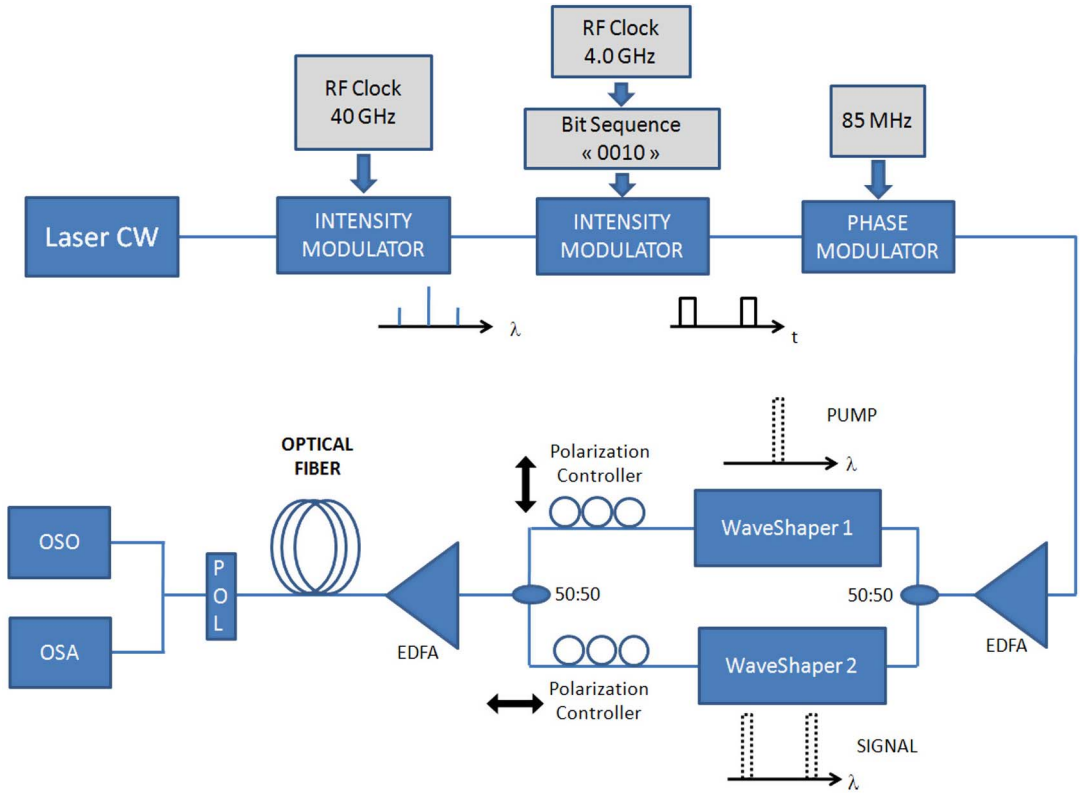

Fig. 9. (Color online) Experimental setup. EDFA, erbium-doped fiber amplifier; POL, polarizer; OSO, optical sampling oscilloscope; OSA, optical spectrum analyzer.

optical spectrum analyzer and a high bandwidth optical sampling oscilloscope (EXFO PICOSOLVE), respectively.

In the first step, in order to experimentally determine the frequency at which the peak amplification of noise due to the scalar MI (corresponding to peak gain of scalar MI or nonlinear phase-matching condition) is observed, only the pump wave is injected into the fiber. For an average pump power of 22 dBm (corresponding to 28 dBm peak power owing to the 1∶4 duty cycle), our measurements show that the spontaneous scalar MI peaks at a frequency $\nu_{\mathrm{MI}} = 82$ GHz, consistent with the theoretical predictions obtained from the fiber parameters provided by the manufacturer.

In the second part of the experiment, pump and signal waves are injected into the fiber with parallel polarizations. The initial frequency modulation ν was fixed to about half of the scalar MI frequency $\nu = \nu_{\mathrm{MI}}/2 = 40$ GHz, determined in the first part of the experiment. The output spectral and temporal profiles are illustrated in Fig. 10 for a pump power of 19.7 dBm. As can be seen and as predicted by the numerical calculations, one obtains a nearly triangular spectrum [see Fig. 10(b)], containing several harmonics of the initial modulation [25]. In the temporal domain [see Fig. 10(a)], one observes a compression of the initial sinusoidal beating, leading to the generation of pulses at a bit rate equal to the initial frequency modulation (40 GHz).

Finally, the pump and signal waves were injected into the fiber with orthogonal linear polarization states. The pump average power was fixed to 20.5 dBm, whereas the signal power on the orthogonal axis was set to 10.5 dBm. The residual part of the signal wave on the pump axis was measured to be less than −6 dBm.

Figures 11(a) and 11(b) show the temporal and spectral profiles of the light wave at the output of the fiber when the analyzer was oriented parallel to the polarization of the

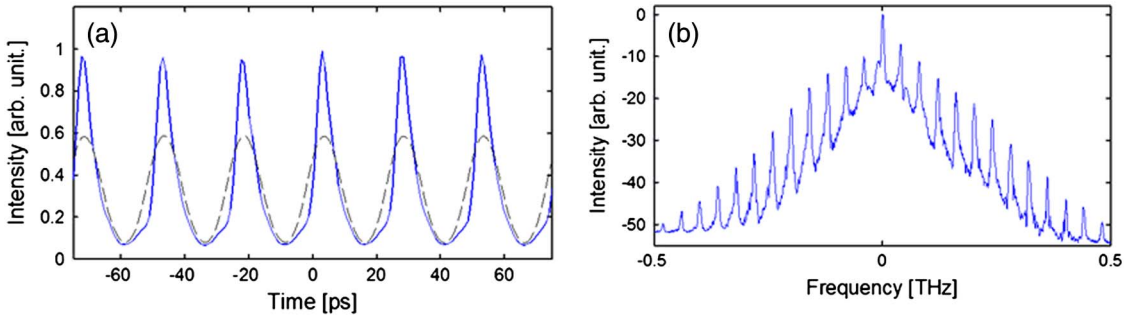

Fig. 10. (Color online) (a) Temporal profiles at the input (dashed curve) and output (solid curve) of the fiber when pump and signal waves have parallel polarization states. (b) Experimental spectrum at the output of the fiber for input parallel polarized pump and signal and for a pump power of 19.7 dBm. Note that the output polarizer was oriented parallel to the pump polarization.

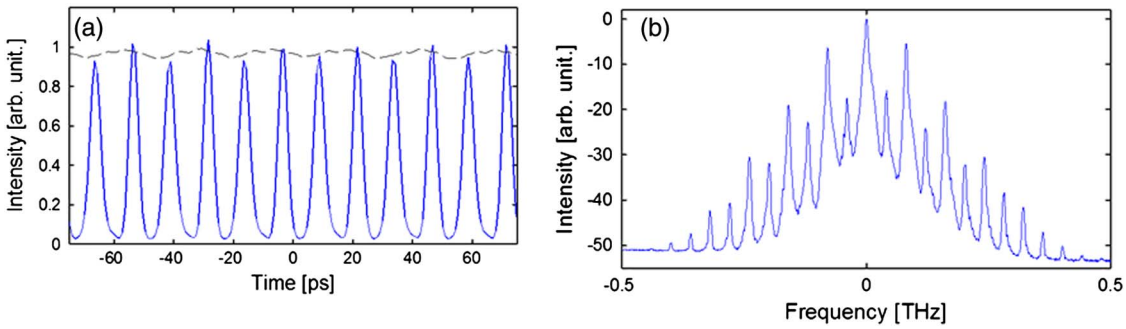

Fig. 11. (Color online) (a) Experimental temporal profiles at the input (dashed curve) and output (solid curve) of the fiber for orthogonal polarized pump and signal waves. (b) Corresponding output experimental spectrum. The output polarizer was oriented parallel to the pump polarization.

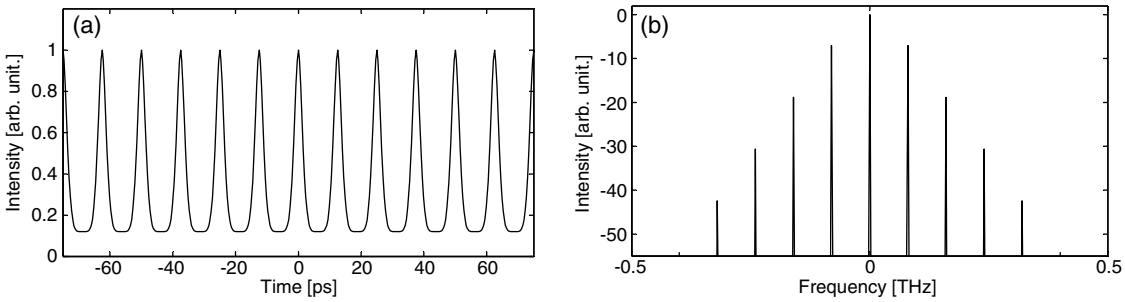

Fig. 12. (a) Temporal and spectral profiles obtained from numerical simulations when the pump and signal waves are injected with orthogonal polarizations.

emerging pump beam. As can be seen and contrary to the previous results shown in Figs. 10 obtained in the parallel polarizations case, the spectrum is now dominated by even harmonics at frequency $k * 80$ GHz $(k = 1, 2, \ldots)$, whereas no exponential growth of the initial modulation is observed at 40 GHz. Indeed, in good agreement with the theoretical predictions of XPolM–MI in Section 2, the generation and amplification of the second harmonic of the modulation is obtained by using an initial frequency modulation fixed at about half of the peak gain frequency of scalar MI: $\nu = \nu_{\mathrm{MI}}/2 = 40$ GHz. As illustrated in Fig. 11(a), in the temporal domain, this spectral feature is associated with the generation of a pulse train at two times the initial signal frequency, corresponding to the second-harmonic repetition rate of 80 GHz, in good qualitative agreement with the numerical predictions of Fig. 12, obtained from the numerical resolution of the VNLSE. The experimental generated pulses have a nearly Gaussian shape with a temporal full width at half-maximum of 4 ps. Note that the residual initial signal harmonics at 40 GHz and −40 GHz around −20 dBm, visible in Fig. 11(b), lead to a weak additional intensity modulation of the pulse train at a period of 25 ps.

4. CONCLUSIONS

In this work we have theoretically predicted and experimentally demonstrated that, by using an orthogonally polarized pump and modulation signal at the input of a low-PMD, randomly birefringent optical fiber, only even harmonics of the modulation are amplified at the fiber output. Indeed, our experiments have shown the generation of an 80 GHz optical pulse train from a 40 GHz modulated signal in the telecom C band by using crossed pump and modulation using a nonzero dispersion-shifted fiber.

ACKNOWLEDGMENT

This work was carried out with support from the Italian Ministry of University and Research (MIUR) through grant contracts 2008MPSSNX and 2009P3K72Z, from the Conseil Régional de Bourgogne, and from the iXCore Foundation. We also thank Prysmian Group for providing the low-PMD nonzero-dispersion-shifted fiber (NZDSF) used in our experiment.

REFERENCES

1. V. I. Bespalov and V. I. Talanov, "Filamentary structure of light beams in nonlinear liquids," Pis'ma Zh. Eksp. Teor. Fiz. **3**, 471–476 (1966) [JETP Lett. 3, 307–310 (1966)].
2. T. B. Benjamin and J. E. Feir, "The disintegration of wave trains on deep water. Part 1: theory," J. Fluid Mech. **27**, 417–430 (1967).
3. L. A. L. Berkhoer and V. E. Zakharov, "Self excitation of waves with different polarizations in nonlinear media," Zh. Eksp. Teor. Fiz. **58**, 903–911 (1970) [Sov. Phys. JETP 31, 486–490 (1970)].
4. V. E. Zakharov and L. A. Ostrovsky, "Modulation instability: the beginning," Phys. D **238**, 540–549 (2009).
5. N. N. Akhmediev, V. M. Eleonskii, and N. E. Kulagin, "Generation of periodic trains of picosecond pulses in an optical fiber: exact solutions," Zh. Eksp. Teor. Fiz. **89**, 1542–1551 (1985) [Sov. Phys. JETP 62, 894–899 (1985)].
6. N. N. Akhmediev and V. I. Korneev, "Modulation instability and periodic solutions of the nonlinear Schrödinger equation," Mat. Fiz. **69**, 189–194 (1986) [Theor. Mat. Phys. 69, 1089 (1986)].
7. N. N. Akhmediev, V. I. Korneev, and N. V. Mitskevich, "N-modulation signals in a single-mode optical waveguide under nonlinear conditions," Zh. Eksp. Teor. Fiz. **94**, 159–170 (1988) [Sov. Phys. JETP 67, 89–95 (1988)].
8. G. Cappellini and S. Trillo, "Third-order three-wave mixing in single-mode fibers: exact solutions and spatial instability effects," J. Opt. Soc. Am. B **8**, 824–838 (1991).
9. S. Trillo and S. Wabnitz, "Dynamics of the nonlinear modulational instability in optical fibers," Opt. Lett. **16**, 986–988 (1991).

10. G. Van Simaeys, Ph. Emplit, and M. Haelterman, "Experimental demonstration of the Fermi–Pasta–Ulam recurrence in a modulationally unstable optical wave," Phys. Rev. Lett. **87**, 033902 (2001).
11. S. Wabnitz and N. N. Akhmediev, "Efficient modulation frequency doubling by induced modulation instability," Opt. Commun. **283**, 1152–1154 (2010).
12. M. Erkintalo, K. Hammani, B. Kibler, C. Finot, N. N. Akhmediev, J. M. Dudley, and G. Genty, "Higher-order modulation instability in nonlinear fiber optics," Phys. Rev. Lett. **107**, 253901 (2011).
13. G. Millot, "Multiple four-wave mixing-induced modulational instability in highly birefringent fibers," Opt. Lett. **26**, 1391–1393 (2001).
14. S. V. Manakov, "On the theory of two-dimensional stationary self-focusing of electromagnetic waves," Zh. Eksp. Teor. Fiz. **65**, 505–516 (1973) [Sov. Phys. JETP 38, 248–253 (1974)].
15. P. K. A. Wai and C. R. Menyuk, "Polarization mode dispersion, decorrelation, and diffusion in optical fibers with randomly varying birefringence," J. Lightwave Technol. **14**, 148–157 (1996).
16. G. J. Roske, "Some nonlinear multiphase reactions," Stud. Appl. Math. **55**, 231–238 (1976).
17. M. G. Forest, S. P. Sheu, and O. C. Wright, "On the construction of orbits homoclinic to plane waves in integrable coupled nonlinear Schrödinger systems," Phys. Lett. A **266**, 24–33 (2000).
18. M. G. Forest, D. W. McLaughlin, D. J. Muraki, and O. C. Wright, "Nonfocusing instabilities in coupled, integrable nonlinear Schrödinger PDES," J. Nonlinear Sci. **10**, 291–331 (2000).
19. O. C. Wright and M. G. Forest, "On the Bäcklund-gauge transformation and homoclinic orbits of a coupled nonlinear Schrödinger system," Phys. D **141**, 104–116 (2000).
20. M. G. Forest and O. C. Wright, "An integrable model for stable: unstable wave coupling phenomena," Phys. D **178**, 173–189 (2003).
21. O. C. Wright, "The Darboux transformation of some Manakov systems," Applied Math. Lett. **16**, 647–652 (2003).
22. O. C. Wright III, "Dressing procedure for some homoclinic connections of the Manakov system," Applied Math. Lett. **19**, 1185–1190 (2006).
23. B. Guo and L. Ling, "Rogue wave, breathers and bright-dark-rogue solutions for the coupled Schrödinger equations," Chin. Phys. Lett. **28**, 110202 (2011).
24. F. Baronio, A. Degasperis, M. Conforti, and S. Wabnitz, "Solutions of the vector nonlinear Schrödinger equations: evidence for deterministic rogue waves," Phys. Rev. Lett. **109**, 044102 (2012).
25. K. Hammani, B. Kibler, C. Finot, P. Morin, J. Fatome, J. M. Dudley, and G. Millot, "Peregrine soliton generation and breakup in standard telecommunications fiber," Opt. Lett. **36**, 112–114 (2011).